Journal of the Nigerian Association of Mathematical Physics
Volume 61 **(July – September** *2021 Issue***), pp55 – 62**

COMPARATIVE STUDY OF THE PREDICTION OF HMF2 USING THREE DIFFERENT IONOSPHERIC MODELS AT AN EQUATORIAL WEST AFRICAN STATION

E J. Oluwadare[1], A. O. Oluwadare[2], O.E Abe[3], O. O. Odeyemi[4], J. O. Adeniyi[5] and E. O. Oyeyemi[4]

[1]Department of Physics, Ajayi Crowther University Oyo, Oyo-State, Nigeria
[2]Department of Physics, Elizade University Ilara-Mokin, Ondo-State, Nigeria
[3]Department of Physics, Federal University Oye-Ekiti, Ekiti-State, Nigeria
[4]Department of Physics, University of Lagos, Lagos-State, Nigeria
[5]Department of Physics, Landmark University Omuaran, Kwara State, Nigeria

Abstract

A good algorithm capable of modelling the ionospheric behaviour accurately is important for a critical space-based application within the Equatorial Ionization Anomaly (EIA) region. In this study, diurnal monthly mean values of the peak height of ionosphere electron density at F2-layer (hmF2) were derived from the ionosonde measurements at Ouagadougou Burkina Faso with geographic latitude 12.4°N, longitude 1.5°W and magnetic dip 1.43°N. The study period covered three solar cycles with different geophysical seasons and condition, it spans through the years 1968 to 1997. Ouagadougou is a station located within the equatorial ionization anomaly (EIA) region of the West African sector. Similarly, the diurnal monthly average of hmF2 was predicted using, empirical models, Artificial Neural Network (ANN) algorithm, NeQuick version 2.0.2 algorithm and the International Reference Ionosphere version 2016 (IRI-2016) algorithm for a period spanning 20 years. In addition, 20 years of solar-geomagnetic data such as solar flux (F10.7), Planetary "A" (Ap) index, plasma wind speed (Vx), plasma wind temperature, interplanetary magnetic field (IMF-Bz) and Disturbed storm time (Dst) with the local time and the day number were used as input variables in the ANN algorithm. The monthly average of sunspot number and solar flux (F10.7) was used as input variables of IRI-2016 and NeQuick2 algorithms respectively. A comprehensive comparative analysis that gives a better agreement with the trend of hmF2 observed was performed on all three models. The results have shown that at equatorial region, ANN produces the highest correlation coefficient (R) of 0.95 with the least residual error mean and standard deviation of (11.67±11.88) km, followed by NeQuick version 2.0.2 having R to be 0.87, residual error with the standard deviation to be 35.63±25.34 km and IRI-2016 has the least correlation coefficient of 0.84 and the most residual error with the standard deviation of (42.76±29.76) km. With the comparative analysis, the study has revealed that ANN could predict accurate and reliable hmF2 that compare well with the actual experimental geophysical conditions.

Keywords*: hmF2; Neural Network; NeQuick 2; IRI-2016; EIA region.*

1. Introduction

A comprehensive study of the ionospheric profile is required to ensure the effective planning, operating, and management of Global Navigation Satellite Systems (GNSS) applications. The system's signals are highly affected by the randomness in the variations of the charged particles (particularly free electrons) density along its path. The density of electron in the ionosphere varies rapidly across the globe due to the non-consistence in the production of the basic important ions (O^+, N^+,

Corresponding Author**:** Oluwadare E.J., Email: ej.oluwadare@acu.edu.ng, Tel: +2348061331133

NO^+, O_2^+ and N_2^+) and electrons by the photo-ionization processes together with their recombination effect to neutral atoms [1-5]. Many researchers have reported that the level of randomness of the electron density in the ionosphere mainly depends on the geographical and geomagnetic coordinates, local time, season, neutral winds and the rapid changes in the solar activity (as measured by F10.7 (solar flux) or sunspot number (SSN)) and magnetic property (measured by the solar wind) of the sun [6-9]. The randomness in the variability in the maximum height of electron density at F-layer (*hmF2*) is more critical at Equatorial Ionization Anomaly (EIA) region where the plasma instability mechanism generates post-sunset plasma bubbles and electron density depletion because the daytime ionization distribution is modified through the fountain effect and develops a crest at around $\pm\ 15^o\ to\ \pm\ 20^o$ magnetic equator and a trough at the magnetic equator during towards the late local noon. The variation of the solar radiation and solar zenith angle could result in the temporal and spatial variations of *hmF2* [10]. They further reported that *hmF2* could range from 350 to 500 km at the equatorial latitudinal regions and 250 to 350 km at the middle latitudes regions depending on the solar activity, local time, season, electric fields and neutral winds.

This *hmF2* parameter is one of the essential ionosphere parameters uses in characterizing the ionosphere over a given region. It is also a key parameter for radio Physics to evaluate ionosphere plasma drift at any point in time. Extensive studies in both theoretical and experimental have been done to understand the active component involves in the evolution of the variability of the ionosphere height. Many regional or global models in empirical, Physics-based or semi-empirical have been developed [5,10-15] to cater for the prediction of the ionosphere electron density height; some of them do better in a quiet geophysical environment like middle latitudes, but either over-estimate or under-estimate at low latitudes. In line with this, International Reference Ionosphere (IRI) is an international project that was set up in the year 1968, sponsored by the Committee on Space Research (COSPAR) and the International Union of Radio Science (URSI), to understand the ionosphere density profile at a given location on the globe [16]. IRI-model has undergone series of versions for optimization in order to cater for the global ionosphere profiling [17-22]. The IRI model was entirely lacking in strength to capture the topside F-layer. The sum of Epstein layers in representing the analytical profiler model (NeQuick model) have been used to reproduce the electron density distribution within the ionosphere [23]. This model was further optimized to cater for the topside F2 region [24-27]. The version of NeQuick model (NeQuick 2) is essentially driven by solar flux F10.7, a special version that has been used in the ionosphere correction algorithm segment of Galileo. International Telecommunication Union-Radio (ITU-R) has adopted NeQuick as a procedure for TEC estimation [25]. The extent to which the NeQuick 2 model allows the creation of a realistic and controlled ionosphere can be found in [28]. However, the *hmF2* being estimated by the NeQuick 2 model still have some shortfall in low latitudes anomaly regions.

Therefore, the ability to model ionosphere height correctly is of great importance in the planning, implementation and operation of ionosphere delay correction algorithm for any global-regional satellite-based navigation and communication systems (GNSS-SBAS, Global Navigation Satellite System-Satellite Based Navigation System), particularly over the low latitudes regions. This study focuses on the methodology of Artificial Neural Network (ANN) to predict *hmF2* at a point within the trough of EIA and compare the output with the IRI-2016 an empirical model and NeQuick version 2.0.2, a profiler. In many cases, ANN has been used to predict the ionospheric parameters. A global model with high forecasting capability of F2-layer (*foF2)* based on neural network has been developed [29]. Neural network has been used to predict the level of ionospheric scintillation over Brazil [30]. Likewise, ANN based-model has been used to predict NmF2 and hmF2 over Indian [31]. ANN output was found to have a better representation of the parameters along the longitudes of their study locations compared with IRI-2016.

2. *hmF2* modelling processes and Neural Networks methodology

To model *hmF2* with the neural network, a ground-based ionosonde data of critical frequencies at E-layer (*foE*), F2-layer (*foF2)* and maximum usable frequency at 3000 Km after reflection (M(3000)) obtained from a station within the trough of EIA in African sector, located at Ouagadougou Burkina Faso, for 20 years was used. The years used spanned from 1969 to 1996, solar cycles 20-22. The vertical ionospheric profile data obtained in MHz were used to compute *hmF2* following the algorithm proposed by [31] given in Eq.(1).

$$hmF2 = \frac{1490MF}{M + \Delta M} - 176 \qquad (1)$$

where $MF = M\sqrt{\frac{0.0196M^2+1}{1.296M^2-1}}$, M is M(3000)/*foF2=(M(3000)F2)*

and $\Delta M = \frac{0.253}{foF2/foE-1.215} - 0.012$

A popular technique used by independent researchers to optimize the NeQuick model in the estimation of *hmF2* is called Dudeney's technique conducted by [27]. In the same way, [10] followed Dudeney methodology to estimate *hmF2*. This technique has also been used in this study.

The artificial neural intelligent network is a special algorithm that fits a set of numeric inputs data during the training process to a set of numeric target. Knowing fully that ionosphere is influence mainly by the solar-geomagnetic conditions and the geophysical dynamism. In this research, the input parameters include the solar-geomagnetic data (solar flux (F10.7), Planetary A-index, plasma wind speed (Vx), plasma wind temperature, interplanetary magnetic field (IMF, Bz) and Disturbed storm time (Dst)), the local time and the day number. While the target parameter is the estimated *hmF2*. The solar-geomagnetic data sets were obtained from the National Aeronautics and Space Administration (NASA) Space Physics Data Facility (http://omniweb.gsfc.nasa.gov/) and the output data set is the estimated *hmF2* as described in Eq. 1. The modelling process is randomly divided into training segment; validation segment and test case segment. 70% of the data used was allotted to the training segment, 15% was used for validation and the remaining 15% of the data was used for a test case. The inputs data were arranged as $x_1, x_2, x_3 \ldots x_n$, and the corresponding weights for the inputs $w_1, w_2, w_3 \ldots w_n$ as shown in the schematic diagram (Fig 1). Though the weight ratio is part of the hidden processes of the network. The weights are assigning to the input parameters during the training process using different algorithms. The neural networks would learn by adjusting the weights connecting different summation of the weights is multiplied by the inputs as shown in the schematic diagram (Fig 1). In addition, the artificial neural network has different layers; the output of the first layer is set to the input of the second layer. During the training process, the network is adjusted according to its error and the output is compared with the target *hmF2* until the predicted values are stabilized. The validation performance at each epoch is evaluated from the connection through to output-size using the root mean square error and regression analysis. Details of the neural network algorithms hidden processes are described in [32,33]. The *hmF2* outputs from the neural network are compared with the *hmF2* estimated from the experimental data and the *hmF2* obtained from NeQuick version 2.0.2 and IRI-2016 models.

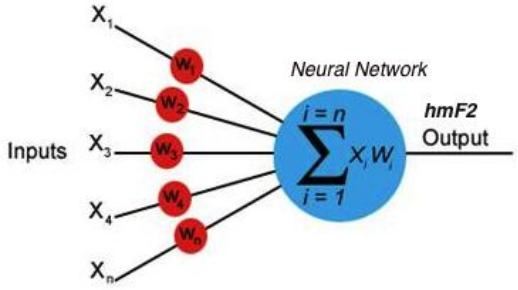

Figure 1: Schematic processes of neural network

3. Results and Discussion

3.1 The regression analysis of the models

Figure 2 presents the result of the regression analysis between the *hmF2* predicted using the artificial neural network and the *hmF2* estimated with the experimental data for the trained, validation and the tested case scenarios. The values of the coefficient of correlation (R) during the training (R= 0.96), validation (R= 0.95) and test case (R=0.95) have shown that all the input parameters in the artificial neural network have a great impact in influencing the evolution of the ionosphere and its height. The result of the regression with the high value of R is an indication that the *hmF2* predicted by ANN is strongly interrelated with the experimental data. On the other hand, Figure 3 shows the regression analysis of the ANN, NeQuick2 and IRI-2016 models together with their residual errors. This Figure describes the interrelationship between the *hmF2* models' outputs and the observed. In the sense that the *hmF2* predicted by ANN gave a better agreement with the *hmF2* observed with correlation (R) of 0.95 and RMSE of 15.85 km followed by NeQuick version 2.0.2 (R=0.87 and RMSE=29.52 km) and IRI-2016 (R=0.84 and RMSE=34.63 km) algorithms. Figure 3 right lower panel illustrates the distribution of the residual error for ANN, NeQuick2 and IRI-2016 models for the 20 years of data used. ANN gives the least mean and the least standard deviation of the residual error$(11.67 \pm 11.87)\ km$, including 75 and 99 percentiles of$(34.77\ and\ 59.07)\ km$ respectively. While NeQuick version 2.0.2, which produces the mean and standard deviation of $(35.87 \pm 24.47)\ km$ 75 and 99 percentiles $(81.45\ and\ 102.41) km$ respectively. The highest residual error among the models evaluated is obtained in IRI-2016 with the mean and standard deviation of $(42.80 \pm 29.59)\ km$, 75 and 99 percentiles $(97.39\ and\ 125.98)\ km$ respectively. Looking at the statistical computation of the regression and the error distribution of the models used, at each instance, the values of the prediction residual error for the mean, standard deviation, 75 percentile, 99 percentile and the RMSE of the ANN remains lower compared with NeQuick 2 and IRI-2016 outputs. This is an indication that ANN could provide an accurate and reliable *hmF2* that compare well with the actual experimental values more than NeQuick 2.0.2 and IRI-2016.

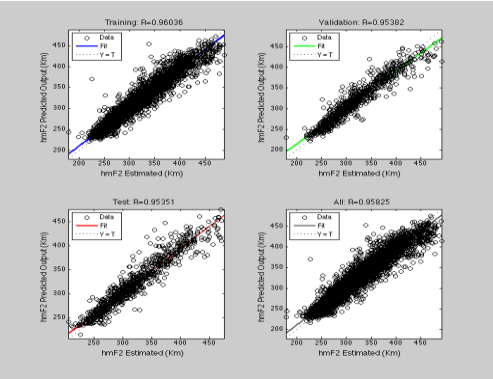

Figure 2: Correlation analysis of the predicted hmF2 and estimated hmF2 for the trained, validation and tested values obtained at Ouagadougou, Burkina Faso.

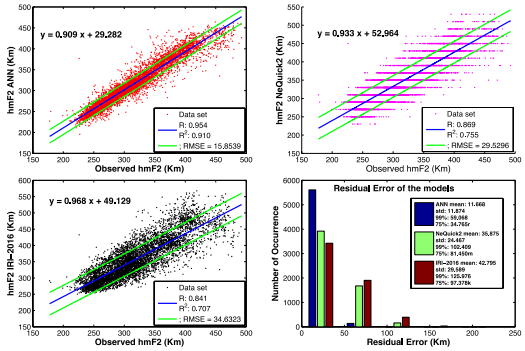

Figure 3: Correlation Analysis of the observed and the predicted hmF2 at Ouagadougou, Burkina Faso: left upper panel (ANN); right upper panel (NeQuick 2); left lower panel (IRI-2016); and right lower panel (Residual Error of the models).

3.2 Influence of Solar Activity on the models

Figure 4a illustrates the comparative analysis of the climatologically monthly mean values for the predicted *hmF2* and the observed during the selected solar minimum years of 1976, 1986 and 1996. The selected years correspond to the solar cycles 20, 21 and 22 with a yearly average of sunspot number 18.34 ± 18.12, 14.74 ± 17.01 and 11.88 ± 18.42 respectively. For clarity, Figure 4b expresses the monthly evolution of the residual error for the selected years. The outputs of the models all follow the same evolutional trend with the observed *hmF2* throughout the year. However, ANN outputs always align with the observed more than NeQuick 2.0.2 and IRI-2016 as clearly observed in Figure 3b, but NeQuick 2.0.2 and IRI-2016 output produce little deviation with some overestimation. The details of the distribution of the residual errors of the models that illustrate the level of deviation from the observed *hmF2* during the minimum years of the cycles considered are presented in the Figure 5. At the minimum solar activity of the solar cycle 20 (1976), average sunspot number of 11.88, ANN model produces the least residual error having the mean, standard deviation, 75 and 99 percentile of $(9.52 \pm 7.90, 23.80\ and\ 36.63)\ km$ respectively. However, NeQuick 2 and IRI-2016 produce quite similar residual error with the mean, standard deviation, 75 and 99 percentile of $(25.24 \pm 18.22, 60.11\ and\ 69.91)\ km\ and\ (27.37 \pm 17.29, 60.52\ and\ 71.46)\ km)$ respectively. Looking at the next minimum solar cycle 21 (1986) with yearly average sunspot number 14.74, ANN has the least error as well with mean, standard deviation, 75 and 99 percentile of $(8.18 \pm 7.03, 21.32\ and\ 31.90)\ km$ respectively. Followed by NeQuick 2 with the mean, standard deviation, 75 and 99 percentile of $(26.39 \pm 20.14, 65.15\ and\ 75.25)\ km$ respectively, while the most error occurred in IRI-2016 model with the mean, standard deviation, 75 and 99 percentile of $(39.68 \pm 24.16, 83.29\ and\ 93.77)\ km$ respectively. Considering minimum year (1996) of the solar cycle 22 with yearly average sunspot number of 11.88, ANN still has the least mean, standard deviation, 75 and 99 percentiles of the residual errors $(15.83 \pm 16.06, 50.10\ and\ 61.82)\ km$ though the error is much great than the residual error obtained in minimum solar cycle 20 and 21. It is as well worth noting NeQuick 2 and IRI-2016 have very close residual errors as follow mean, standard deviation, 75 and 99 percentile $(33.12 \pm 22.83, 75.46\ and\ 92.01)\ km$ and $(33.93 \pm 23.06, 74.25\ and\ 88.41)\ km$ respectively. This means that the algorithms of the two models have some similarity and are essentially driving nearly by the same indices. It is interesting to note that the statistics of the residual errors for all the minimum solar activity of the cycles considered are below the mean errors

obtained for the whole 20 years, except ANN model during the solar cycle 22 (1996). The ANN output residual mean, standard deviation, 75 and 99 percentile $(15.83 \pm 16.06, 50.10\ and\ 61.82)\ km$ errors are found above the ANN output residual mean, standard deviation, 75 and 99 percentile $(11.67 \pm 11.87, 34.77\ and\ 59.07)\ km$ errors for the whole 20 years considered.

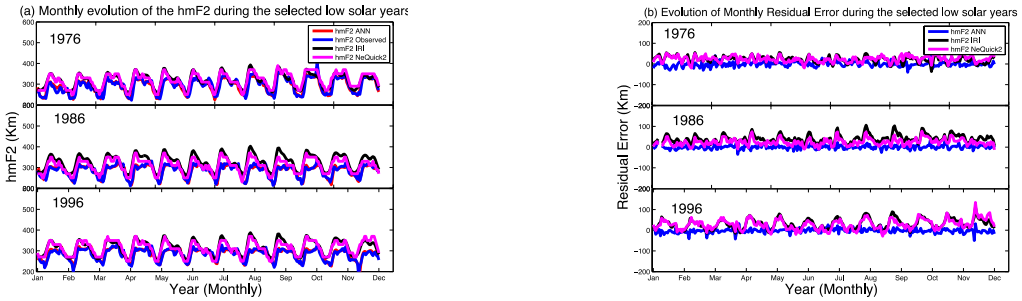

Figure 4: Monthly evolution of the observed and predicted hmF2 for the selected low solar years and their residual errors. The left hand side is the absolute hmF2 and right hand side contains the residual errors of the models.

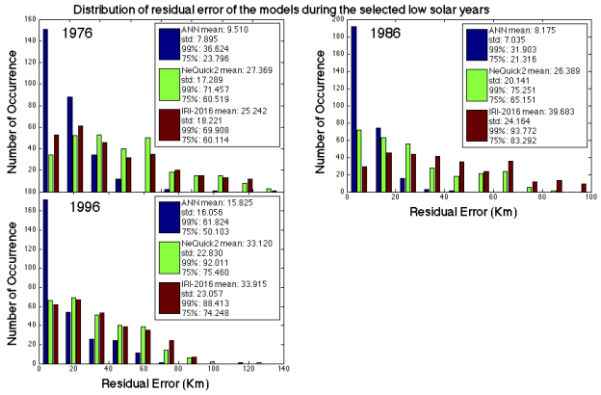

Figure 5: Histogram distribution of the residual error of the models during the selected low solar years.

Figure 6a describes the monthly evolution of the *hmF2*, Figure 6b shows the evolution of the residual error along the years while Figure 7 illustrates the distribution of the residual error obtained from the models during the maximum solar activity of years (1969, 1979 and 1989) for the cycles 20, 21 and 22 with the yearly average of the sunspot number and their standard deviation of 149.37 ± 22.59, 220.30 ± 23.77 and 210.38 ± 36.30 respectively. It is cleared from Figure 6a that all the models are consistence in following the trend of evolution of the observed *hmF2* just like during the solar minimum activities considered. However, in the year 1969 the *hmF2* model output by ANN is more aligned with the observed, followed by IRI-2016 and NeQuick 2. But for years 1979 and 1989 ANN output is most aligned with the observed, followed by NeQuick 2 and IRI-2016. The better correspondent in ANN output over other models could be because it does not have any saturation point for the input indices used unlike NeQuick 2 that saturates at sunspot number 150 and solar flux 193. Figure 7 illustrates the distributions of the residual error at the maximum phase of the solar cycles considered, the mean of the residual error and its standard deviation together with 75 and 99 percentile are less at maximum phase of solar cycle 20 ANN $(11.10 \pm 9.64, 24.99\ and\ 51.28)\ km$, NeQuick 2 $(39.11 \pm 21.78, 77.82\ and\ 94.32)\ km$ and IRI-2016 $(33.94 \pm 21.05, 73.95\ and\ 85.08)\ km$ respectively, followed by cycle 21 ANN $(13.81 \pm 12.20, 41.90\ and\ 56.70)\ km$, NeQuick 2 $(38.70 \pm 24.62, 84.60\ and\ 103.53)\ km$ and IRI-2016 $(50.05 \pm 28.75, 98.96\ and\ 115.60)\ km$ while the maximum error is obtained at the cycle 22 for ANN$(15.82 \pm 15.86, 49.56\ and\ 72.00)\ km$, NeQuick $(43.81 \pm 32.25, 107.83\ and\ 120.58)\ km$ and IRI$(76.32 \pm 48.61, 153.30\ and\ 176.81)\ km$. This is almost corresponding to the results obtained during the minimum phase of each cycle, where the most errors were obtained at the cycle 22 and are well found above the average error of the whole period considered. These results show that ANN produces the least error compared with other models and the errors increases with the level of solar activity and the level of its fluctuations. The irregular behaviour of the sun at the cycle 22 as indicated by the standard deviation 18.42 for the minimum phase and 36.30 for the maximum phase of cycle, a bit above other cycles, must have accounted for the highest error obtained in the cycle. Since the models are driving essentially by the solar indices. Comparatively, the results of the statistics have shown that in all geophysical conditions, ANN output gives a better *hmF2* that correspondent well with the observed, followed by NeQuick 2 and least in IRI-2016.

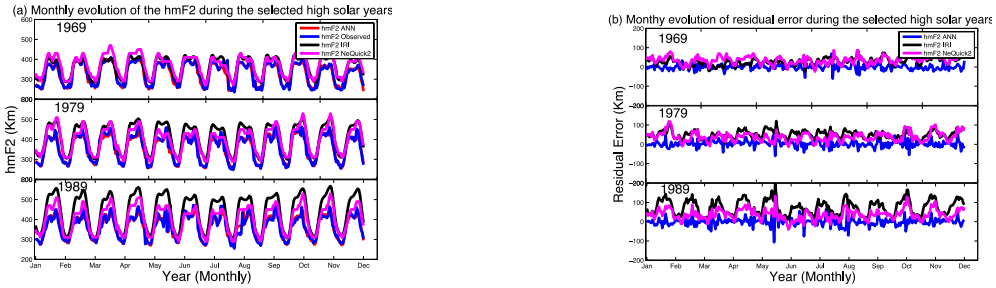

Figure 6: Monthly evolution of the observed and predicted hmF2 for the selected high solar years and their residual errors. The left hand side is the absolute hmF2 and right hand side contains the residual errors of the models.

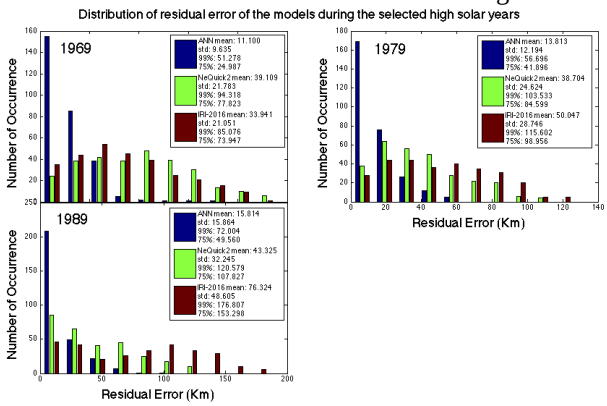

Figure 7: Histogram distribution of the residual error of the models during the selected high solar years.

3.2 Diurnal and Seasonal effect on the models

Figure 8 illustrates the seasonal evolution of the *hmF2* during the selected low solar years {upper panel (year 1976), middle panel (1986) and lower panel (1996)} and high solar activity considered {upper panel (year 1969), middle panel (1979) and lower panel (1989)}. The Figure affirms the consistence alignment of ANN prediction with the observed values irrespective of the level of solar activity and season. The daytime and nighttime are well captured by the network in all the seasons. However, the NeQuick 2 and the IRI-2016 output deviated a bit and this is more glaring during the high solar year of 1989 where the residual error of the IRI-2016 reached ~100 km at the daytime and NeQuick 2 ~70 km. Looking closely at the daily variations of the models' output with the observed, Figure 9 describes the diurnal trend of the models. Again, no much difference was observed at ANN output

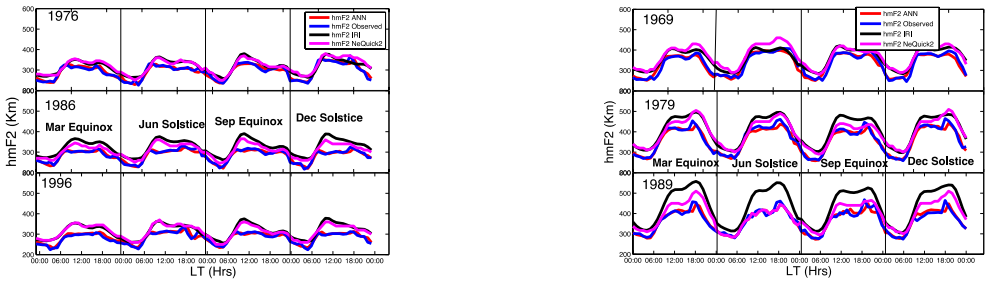

Figure 8: Seasonal diurnal evolution of the hmF2 during the selected low solar years {left, upper panel (year 1976), middle panel (1986) and lower panel (1996)} and high solar years {right, upper panel (year 1969), middle panel (1979) and lower panel (1989)}

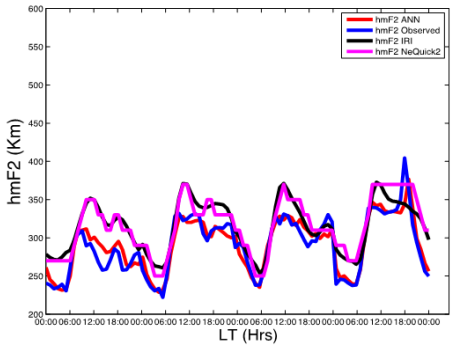

Figure 9: Diurnal evolution of the hmF2 for a selected nominal day in year 1976.

4 Conclusion

The study has found ANN to have the output that better represent hmF2 in all the solar activities and seasons. It is interesting to note that NeQuick 2 and IRI-2016 essentially predicted the same trend with the residual mean and standard deviation error of $(36 \pm 26) km\ and$ respectively. However, both NeQuick 2 and IRI-2016 overestimate *hmF2* in the region considered.

References

[1] Hedin, Alan E. 1987 "MSIS-86 Thermospheric Model" Journal of Geophysical Research: Space Physics Vol. 92, IssueA5 pp 4649-4662 doi:10.1029/JA092iA05p04649

[2] Marcel Nicolet 1965 "Ionospheric processes and nitric oxide" Journal of Geophysical Research Vol.70, Issue3 pp 691-701 doi:10.1029/JZ070i003p00691

[3] Rishbeth, Henry and Owen K. Garriott. 1969. "Introduction to Ionospheric Physics." Vol. 14, Pages iii-vii, 1-331.

[4] Titheridge, J.E 1997 "Model results for the ionospheric E region: solar and seasonal changes. Annales Geophysicae 15, pp 63–78. doi:10.1007/s00585-997-0063-9

[5] Titheridge, J. E. 2000. "Modelling the peak of the ionospheric E-layer", Journal of Atmospheric and Solar-Terrestrial Physics, Vol. 62, Issue 2, pp 93-114, ISSN 1364-6826, doi:10.1016/S1364-6826(99)00102-9

[6] Chen, T., Y. Zhang, and B. Rossow, w. 2000. "Sensitivity of Atmospheric Radiative Heating Rate Profiles to Variations of Cloud Layer Overlap". Journal of Climate, pp 2941–2959 doi:10.1175/1520-0442(2000)013<2941:SOARHR>2.0.CO;2.

[7] Oluwadare E.J., Adeniyi J.O., Ademula I.A., Oladipo O.A., Olawepo A.O., (2015). Latitudinal Dependence of Vertical Total Electron Content in the Equatorial and Low Latitude Regions of the African Sector. URSI- NG Conference Proceedings. pp 21 – 28. Publisher: Physics Department, University of Ilorin and International Union of Radio Science – Nigeria.

[8] Oluwadare, E, J. 2017. "Latitudinal Variation of Total Electron Content in the East African Sector and Validation of International Reference Ionosphere Model." Ph.D Thesis, University of Ilorin, Nigeria.

[9] Rabiu, A, B, I. Mamukuyomi, A, and O. Joshua, E. 2007. "Variability of Equatorial Ionosphere Inferred from Geomagnetic Field Measurements Variability of Equatorial Ionosphere Inferred from Geomagnetic Field Measurements." Bulletin of the Astronomical Society of India.

[10] Hoque, M. M. and N. Jakowski. 2012. "A New Global Model for the Ionospheric F2 Peak Height for Radio Wave Propagation." Annales Geophysicae, Vol. 30, Issue 5, 2012, pp.797-809.

[11] Bilitza, Dieter, R. Eyfrig, and N. M. Sheikh. 1979. "A Global Model for the Height of the F2-Peak Using M3000 Values from the CCIR Numerical Map." ITU Telecommunication 46:549–53.

[12] Bradley, P. A. and J. R. Dudeney. 1973. "A Simple Model of the Vertical Distribution of Electron Concentration in the Ionosphere." Journal of Atmospheric and Terrestrial Physics, Vol. 35, Issue 12, pp 2131-2146, ISSN 0021-9169, doi:10.1016/0021-9169(73)90132-3.

[13] Dudeney, J. R., Rodger, A. S., and Jarvis, M. J. 1983, "Radio studies of the main F region trough in Antarctica", Radio Sci., 18(6), pp 927– 936, doi:10.1029/RS018i006p00927.

[14] Shimazaki, T. 1955. "World-Wide Daily Variations in the Height of the Maximum Electron Density of the Ionospheric F2 Layer." J. Radio Res. Labs., Japan 2(85).

[13] Rawer, K., Bilitza, D., and Ramakrishnan, S. 1978, "Goals and status of the International Reference Ionosphere", *Rev. Geophys.*, 16(2), pp 177– 181, doi:10.1029/RG016i002p00177.

[16] Bilitza, Dieter. 1990. International Ionosphere Reference 1990.

[17] Bilitza, Dieter. 2001. "International Reference Ionosphere 2000 of Ionospheric It Was and the F Peak down To." Radio Science 36(2) pp 261–275.

[18] Bilitza1 Dieter,, David Altadill, Yongliang Zhang, Chris Mertens, Vladimir Truhlik, Phil Richards, Lee-Anne McKinnel and Bodo Reinisch 2014. "The International Reference Ionosphere 2012 – a Model of International Collaboration" J.Space Weather Space Clim. 4 (A07) doi:10.1051/swsc/2014004.

[19] Bilitza, Dieter, Steven A. Brown, Mathew Y. Wang, Jonas R. Souza, and Patrick A. Roddy. 2012. "Measurements and IRI Model Predictions during the Recent Solar Minimum." Journal of Atmospheric and Solar-Terrestrial Physics, Vol. 86, pp 99-106, ISSN 1364-6826, doi:10.1016/j.jastp.2012.06.010.

[20] Bilitza, Dieter., K. Rawer, L. Bossy, and T. Gulyaeva. 1993. "International Reference Ionosphere - Past, Present, and Future: II. Plasma Temperatures, Ion Composition and Ion Drift." Advances in Space Research 13(3):15–23.

[21] Bilitza, Dieter. and B. W. Reinisch. 2008. "International Reference Ionosphere 2007: Improvements and New Parameters." Advances in Space Research 42(4):599–609.

[22] Giovanni, G. Di and S. M. Radicella. 1990. "An Analytical Model of The Electron Density Profile In The Ionosphere." Advances in Space Research, Vol. 10, Issue 11, pp 27-30, ISSN 0273-1177, doi:10.1016/0273-1177(90)90301-F.

[23] Coïsson, P., Sandro M. Radicella, R. Leitinger, and B. Nava. 2006. "Topside Electron Density in IRI and eQuick : Features and Limitations." Adv. Space Res. 37, pp 937–942.

[24] Nava, B., P. Coïsson, and S. M. Radicella. 2008. "A New Version of the NeQuick Ionosphere Electron Density Model." Journal of Atmospheric and Solar-Terrestrial Physics 70(15), pp 1856–1862.

[25] Radicella, Sandro M. 2009. "The NeQuick Model Genesis, Uses and Evolution." Ann. Geophys. 52(3-4), pp 417–4122.

[26] Radicella, Sandro and Man-lian Zhang. 1995. "The Improved DGR Analytical Model of Electron Density Height Profile and Total Electron Content in the Ionosphere." Ann. Geophys 38(1) doi:10.4401/ag-4130.

[27] Brunini C, Azpilicueta F, Gende M, Camilion E, Aragón Ángel A, Hernandez-Pajares M, Juan M, Sanz J and Dagoberto Salazar. 2011. "Ground- and Space-Based GPS Data Ingestion into the NeQuick Model." Journal of Geodesy, 85(12), pp 931–939.

[28] Oyeyemi, E. O. and A. W. V Poole. 2005. "On the Global Model for f o F 2 Using Neural Networks." Radio Sci., 40, RS6011, doi:10.1029/2004RS003223.

[29] De Lima, G. R. T., S. Stephany, E. R. De Paula, I. S. Batista, and M. A. Abdu. 2015. "Prediction of the Level of Ionospheric Scintillation at Equatorial Latitudes in Brazil Using a Neural Network." Space Weather 13(8), pp 446–57.

[30] Sai Gowtam, V. and S. Tulasi Ram. 2017. "An Artificial Neural Network-Based Ionospheric Model to Predict NmF2 and hmF2 Using Long-Term Data Set of FORMOSAT-3/COSMIC Radio Occultation Observations: Preliminary Results." Journal of Geophysical Research: Space Physics 122(11), pp 11,743- 11,755. doi:10.1002/2017JA024795.

[31] Dudeney, J. R. 1983. "The Accuracy of Simple Methods for Determining the Height of the Maximum Electron Concentration of the F2-Layer from Scaled Ionospheric Characteristics." Journal of Atmospheric and Terrestrial Physics 45(8–9), pp 629–640.

[32] Haykin, Simon. 1994. "Neural Networks - A Comprehensive Foundation. Second Edition". Pearson Education, Inc, ISBN-13: 9780132733502.

[33] Bilitza, Dieter, K. Rawer, L. Bossy, and T. Gulyaeva. 1993. "International Reference Ionosphere Past, Present, And Future: I. Electron Density." Advances in Space Research 13(3), pp 3–13.